International Journal of Precision Engineering and Manufacturing-Green Technology
https://doi.org/10.1007/s40684-021-00362-3

Online ISSN 2198-0810
Print ISSN 2288-6206

REGULAR PAPER

Microscale Surface Patterning of Zirconia by Femtosecond Pulsed Laser Irradiation

Yuka Yamamuro[1] · Tomotaka Shimoyama[2] · Jiwang Yan[1]

Received: 30 December 2020 / Revised: 15 April 2021 / Accepted: 3 May 2021

Abstract
Irradiation of yttria-stabilized zirconia (YSZ) was performed by a femtosecond pulsed laser to investigate the feasibility of V-shaped groove microstructure fabrication. Firstly, fundamental characteristics of microgroove fabrication was investigated by varying scanning speed of laser and number of scans. Higher scanning speed resulted in a smooth surface without any debris adhesion. By increasing number of scans, the cross-sectional profile of the microgroove became a well-defined V shape, and the taper angle of the V-shaped groove can be precisely controlled by laser scanning speed. Moreover, the laser-induced phase transformation of YSZ was characterized, and it was found that the monoclinic ratio after irradiation decreased in comparison with original YSZ surface, indicating improved strength and toughness. TEM cross-sectional observation of the microgrooves was performed and tetragonal phase was detected independent of locations. Finally, micro pyramid structures were created on the YSZ surface by perpendicularly crossing the laser scan directions. The resulting surface showed a drastic change in surface wettability. These findings demonstrated the possibility of generating precise complex microstructures on YSZ surface with high functionality and low subsurface damage, presenting great potential of wide applications in industry.

Keywords Microstructure · Surface patterning/texturing · Zirconia · Femtosecond pulsed laser · Phase transformation · Ceramic material

1 Introduction

Yttria-stabilized zirconia (YSZ) is a fine ceramic material which has high strength, wear resistance, biocompatibility, and unique aesthetic effects [1–4]. Due to these excellent material properties, YSZ is widely used in many applications such as dental implants, biomaterial components, solid oxide fuel cells, sensors, and optical fiber connectors. In recent years, the demand for YSZ is increasing in various fields [5, 6].

For exploring new applications and improving capabilities of existing applications of zirconia materials, extensive research on microscale surface patterning/texturing has been conducted in recent years. Micro and nanostructured surfaces have been found to greatly improve biomaterials bioactivity and stem cells osteogenic differentiation [7, 8]. For dental implants, micro groove fabrication on the components shows good biocompatibility with mucous membrane and somatic cells. Carvalho et al. found that the osteoblast precursor cell behavior changes significantly on the micro textured zirconia surfaces [9]. Moreover, surface structures with parallel grooves or pyramid spikes can evidently improve surface functionality, such as wettability, and enable reduction of friction and optical reflection [10–12]. Therefore, high-precision microscale surface patterning/texturing technology is necessary for enhancing surface functionality and exploring new applications of zirconia products.

However, YSZ is hard and brittle, which makes it difficult to be precisely machined into the desired shape with high surface quality. Conventional methods such as cutting, grinding and polishing can only be used for machining flat or low aspect ratio curved surfaces [13–15], while they are not suitable for the fabrication of complicated surfaces with high aspect ratios and microscale surface structures. In addition,

This paper was presented at PRESM2020.

✉ Jiwang Yan
yan@mech.keio.ac.jp

[1] School of Integrated Design Engineering, Graduate School of Science and Technology, Keio University, Hiyoshi 3-14-1, Kohoku-ku, Yokohama 223-8522, Japan

[2] Inorganic Materials Research Laboratory, TOSOH Corporation, Hayakawa 2743-1, Ayase 252-1123, Japan

Published online: 17 May 2021

YSZ is chemically stable. Thus, it is difficult to use chemical etching for surface structuring [16].

In recent years, laser processing has been applied to generate high aspect ratio surface structures [17]. It has been used for surface structuring on various types of engineering materials such as metallic materials, ceramics, and semiconductors [18–21]. Laser processing has three major advantages over mechanical processing methods. First, it is a noncontact method and its machining ability is independent of material hardness, thus there is no tool wear problems. Second, it has high flexibility of machining depth/path control through galvanometer scanning mirrors. Thus, surface structures with complex shapes can be fabricated over a large area in a short time with low energy consumption. Third, laser processing does not need coolants/lubricants which are generally used in conventional mechanical processes and does not emit chemical wastes, thus has little impact on environment. From these viewpoints, laser surface structuring is energy-efficient and eco-friendly, thus contributes greatly to future green manufacturing society.

Under normal pressure and temperature conditions, YSZ consists of tetragonal phase. However, the tetragonal phase transforms partially into a low-strength monoclinic phase due to stresses and thermal effects during machining processes [22, 23]. In case of laser machining, thermal damage is a critical problem for YSZ. The phase transformation from tetragonal phase to monoclinic phase was reported in many previous studies. For example, when using nano and picosecond lasers, a melted layer was found on the irradiated surfaces [24–27] and the machined area showed a high proportion of monoclinic phase [28]. In contrast, laser ablation by femtosecond pulses is known to be an effective method to minimize the thermal effect. This is due to the time taken for heat transfer to occur is much longer than the pulse width. Delgado et al. fabricated microstructures such as parallel grooves and porous surfaces on zirconia dental implants without any phase transformation [29]. They pioneered the possibility of microscale surface fabrication by femtosecond pulsed laser irradiation on zirconia with low thermal damage to the material. In recent years, microscale surface patterning/texturing of zirconia was studied by many other researchers and the feasibility of ultrashort pulse to eliminate phase transformation on irradiated surface was confirmed [29, 30].

However, up to date, there is no literature focusing on laser generation of high aspect ratio V-shaped grooves, which is a kind of important microstructures having various applications, such as dental implant surface wettability control and optical fiber alignment in fiber connectors. The effect of laser parameters on taper angles and groove shapes has not been clarified. Moreover, whether thermal effect exists or not inside such V-shaped grooves during femtosecond pulsed laser irradiations is still a question. Laser-induced phase transformation behavior of YSZ during generating high aspect ratio grooves is also unclear.

In this study, we performed microscale surface patterning of YSZ by femtosecond pulsed laser irradiation and investigated the fundamental characteristics of V-shaped groove formation. The effects of laser parameters on groove surface morphology and taper angle development were clarified. Furthermore, the laser-induced phase transformation behavior of YSZ in generating deep grooves was investigated, and processing parameters for suppressing the phase transformation were explored.

2 Experiments

The laser used in this study was PHAROS-08-600-PP, an Yb:KGW laser made by Light Conversion, UAB, Lithuania. The laser wavelength was 514 nm and the repetition frequency was 100 kHz. The energy density of the laser beam had a Gaussian distribution. The laser spot diameter was 15 μm and the focal length was 70 mm. The laser beam was scanned in two dimensions using a galvanometer scanner system under control of a programs created by the Winlase software. The laser beam was focused onto the workpiece using an fθ lens.

Fully sintered YSZ containing 3 mol% Y_2O_3 for stabilization made by Tosoh Corporation was used as workpiece. The sample was cut into a rectangular plate with dimensions of 23 mm × 23 mm × 5 mm. The sample surface was as sintered without polishing. The grain size was about 500 nm. The experimental conditions are shown in Table 1, and the irradiation schemes in Fig. 1.

First, line-scan irradiation was performed to fabricate microgrooves. Then, micro pyramid structures were fabricated by crossing of the microgrooves generated along two perpendicular directions. After the experiment, the sample

Table 1 Experimental conditions

Laser medium	Yb:KGW
Wavelength [nm]	514
Spot size: d [μm]	15
Pulse width [fs]	256
Repetition frequency: f [kHz]	100
Scanning speed: v [mm/s]	1.0, 10, 50, 100, 500, 1000
Laser fluence: F [J/cm^2]	5.0
Number of scans: N	1–10
Scanning pitch [μm]	30, 40, 50
Atmosphere	Air

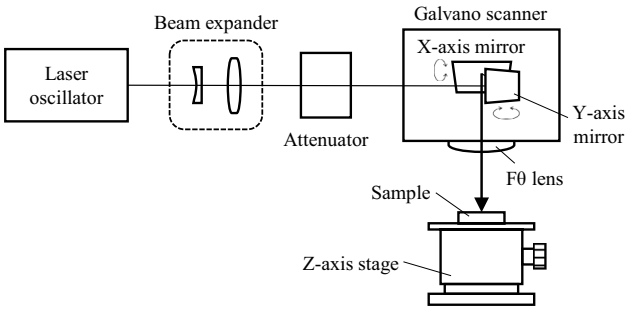

Fig. 1 Experimental setup of laser optical system

was cleaned by an ultrasonic vibration cleaner in ethanol for 10 min to remove debris attached on the surface.

After laser irradiation, the surface morphologies of the samples were observed by a scanning electron microscope (SEM), Inspect F50, made by FEI Company, USA. The groove profiles and depth of irradiated area were measured by a laser microscope, OLS4100, made by Olympus Corporation, Japan. Phase transformation was evaluated by a laser micro-Raman spectrometer, InVia Raman Microscope, made by Renishaw plc., UK. The beam diameter of the Raman spectrometer is 1 μm. To observe the cross-sections of grooves, a focused ion beam (FIB) equipment was used to cut and thin the sample. Then the sample was observed using a transmission electron microscope (TEM), Tecnai G2, made by FEI Company, USA. Selected area electron diffraction (SAED) was used to evaluate the phase transformation in subsurface region. To evaluate the surface wettability, the contact angle of the surface was measured by a contact angle meter, Simage Entry 5, made by Excimer Inc., Japan.

3 Results and Discussion

3.1 Surface Morphology

Figure 2 shows SEM photographs of YSZ surfaces irradiated at different scanning speed and number of scans. For single-scan irradiation ($N=1$), a large amount of debris was stuck on the groove surface at a low scanning speed (10 mm/s), which was hardly removed by ultrasonic vibration cleaning after irradiation (Fig. 2a). However, by increasing the scanning speed to 50 mm/s, debris were removed from the groove surface completely (Fig. 2b). In addition, HSFL, namely high spatial frequency LIPSS (laser-induced periodical surface structures) [31], were generated at the bottom of the groove at 100 mm/s (Fig. 2c). When $N=10$, there was no debris adhesion in spite of laser scanning speed (Fig. 2d–f). The surfaces were very smooth, and the bottoms of the V-shaped grooves could be clearly identified. At all scanning speeds, there were no melt layers and cracks on the surfaces. Moreover, there were no pileups caused by the pushing up of the melt flows of materials as seen in grooves generated by nanosecond pulse lasers [32].

Figure 3 shows changes in groove depth for different number of scans and scanning speeds, respectively. The groove depth was dramatically decreased as scanning speed increases, especially for scanning speeds higher than 100 mm/s. This is because of the difference in incident laser pulse number per area on the material. At 50 mm/s, the laser pulse overlap rate is more than 90%; while the overlap rate decreased to 58% at 500 mm/s, and 22% at 1000 mm/s, respectively. At a higher scanning speed, only a small number of pulses are irradiated on a given area.

3.2 Groove Slope Angle

The cross-sectional profiles of microgrooves generated at different scanning speeds and number of scans are shown in Fig. 4. All grooves have clear edges at the ablation boundaries without piled-up materials. For a small number of scans ($N=1\sim2$) at 50 and 100 mm/s, grooves were ablated with Gaussian shapes due to the laser energy distribution. By increasing the number of scans to $N=6$, groove depth became deeper with a similar groove width. After a certain number of scans ($N=6$), a sharp V-shaped groove was formed, which did not change greatly by further increasing the number of scans. At a scanning speed of 500 mm/s, the groove depth increased gradually, but V-shaped groove was not formed even if at high number of scans.

To investigate the mechanism of V-shaped groove formation, the slope angles of microgroove walls were measured based on the cross-sectional profiles shown in Fig. 4. The changes in slope angle with number of scans are shown in Fig. 5. Slope angles increased by increasing number of scans for all scanning speeds. At 10, 50 and 100 mm/s, the angle increased dramatically in the range of $N=1\sim2$, then converged gradually and reached 76.3°, 75.3° and 70.4°, respectively at $N=10$. On the other hand, in the case of 500 mm/s, the slope angle increased continuously and finally became 39.7° after 10 laser scans, which is close to the angle of grooves at $N=1$ and a scanning speed of 100 mm/s. Comparing among different laser scanning speeds, it is clear that the final V-shaped groove angle at $N=10$ was different. The lower scanning speed, the larger the slope angle. It indicated that the groove slope angle can be adjusted by varying laser scanning speed and number of scans.

The effect of laser scanning speed and number of scans on the groove slope angle can be discussed from the dynamic change of cross-sectional surface profile during multiple laser irradiation. When a Gaussian laser beam is irradiated onto a substrate, the incident beam is absorbed by the material and ablation occurs. Thus, the ablated profile shows a curved shape corresponding to the laser energy distribution.

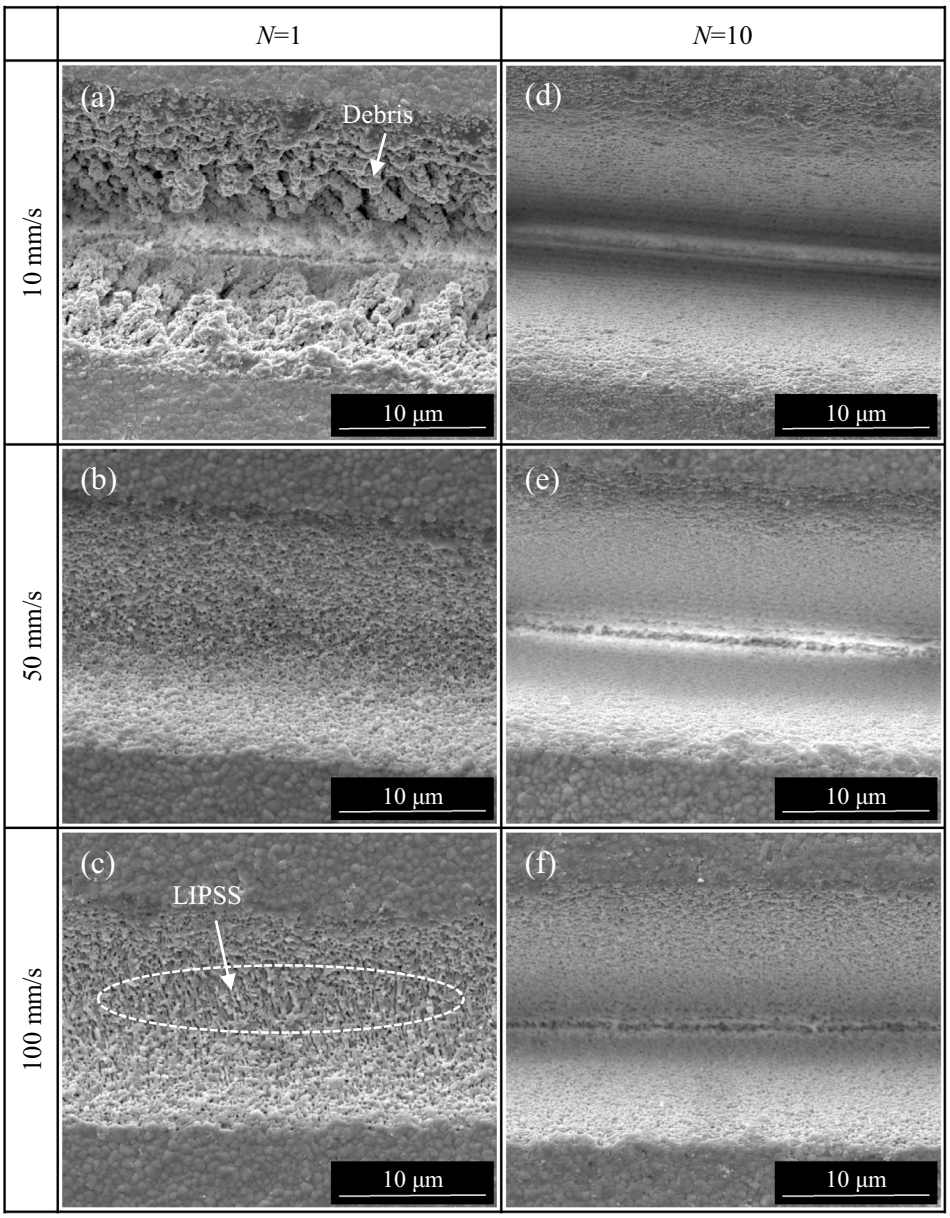

Fig. 2 SEM images of grooved surface under different scan speeds and number of scans

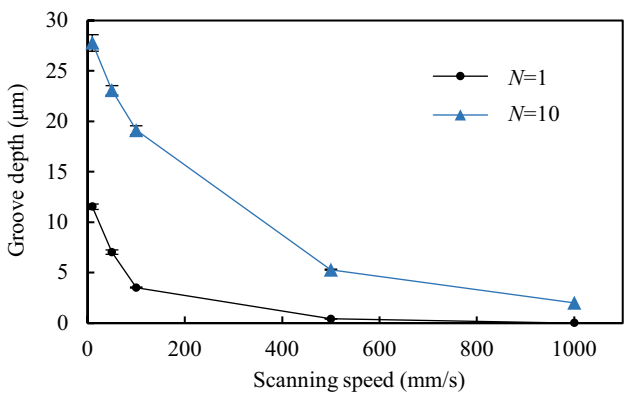

Fig. 3 Change in groove depth with scanning speed and number of scans

With repeated irradiations, the groove bottom becomes deeper and this leads to a defocusing effect at the irradiated surface.

Laser fluence is calculated by dividing the incident power by the laser spot area as the following equation:

$$F = \frac{E}{A} \tag{1}$$

where E is the average laser power of one pulse and A is the spot size, respectively. However, by repeating the laser scan, area A is changed due to groove formation. To consider the laser incident area on the groove wall, beam spot area A_{taper} at a wall with a tilted angle θ can be written by the following equation [17].

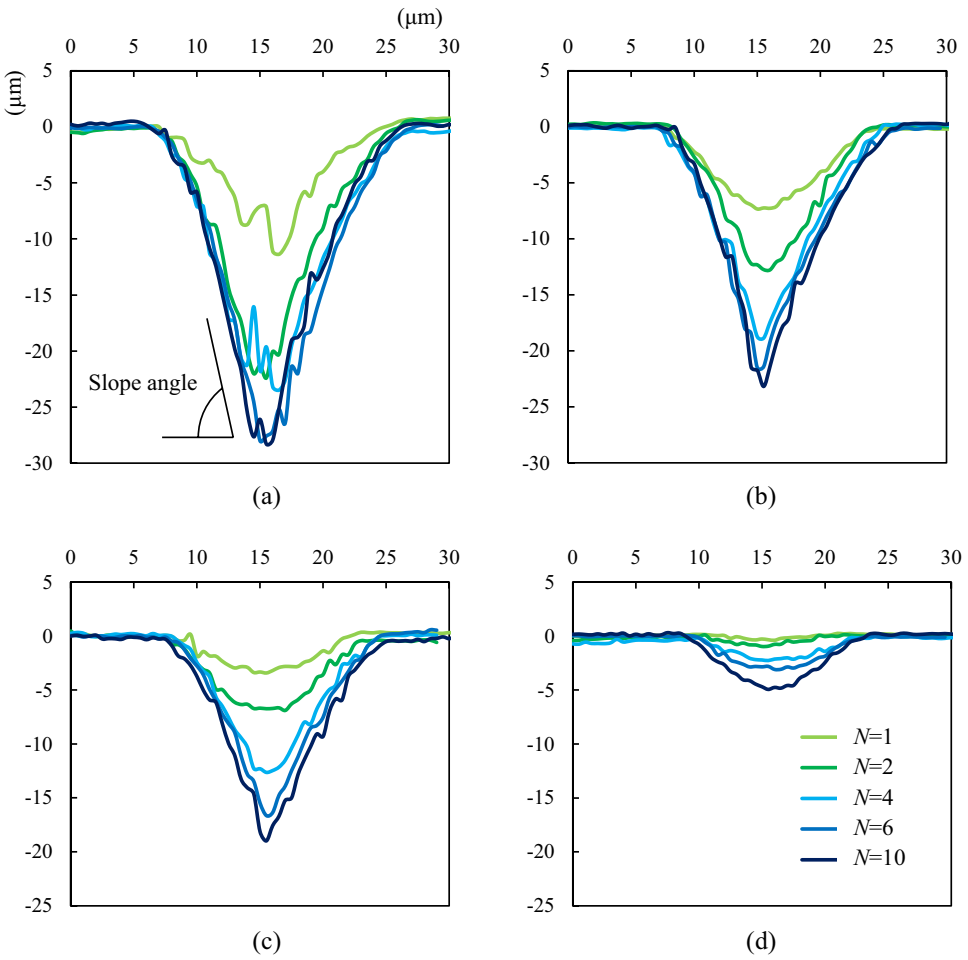

Fig. 4 Cross-sectional profiles of microgrooves irradiated under various conditions: **a** 10 mm/s, **b** 50 mm/s, **c** 100 mm/s and **d** 500 mm/s

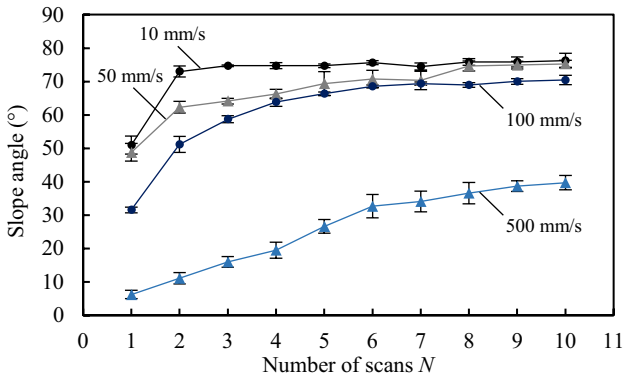

Fig. 5 Change in slope angle with number of scans at various scanning speeds

$$A_{\text{taper}} = \frac{A}{\cos\theta} \tag{2}$$

In Eq. (2), for simplicity, it was assumed that the laser spot size does not change with the groove depth. The Rayleigh length of the laser beam used in this study is more than 300 μm, while the groove depth is about 30 μm, sufficiently small compared to the Rayleigh length, the change in spot size with the change in groove depth is negligibly small. Another assumption is that Eq. (2) is used for modeling the final slope angle of the V-groove after multiple irradiations to consider the limitation of the change in the angle. In the case of a small number of scans, namely, in the early stage of grooving, the microgroove profile is curved, not V-shaped, hence slope angle is not constant at the sides and the bottom, thus the Eq. (2) is not applicable. When the microgroove grows into V-shaped as the laser irradiation is repeated, and finally slope angle can be predicted using the equation. As shown in Fig. 6, the incident laser fluence decreases by increasing θ. It can be considered that the tilted surface of the V-shaped groove cannot absorb adequate laser fluence for further deepening the groove when the slope angle increased to a critical value.

A V-shaped groove is formed after multiple irradiations and the slope angle is converged. By increasing the number of scans, the groove wall is not machined anymore and only the bottom becomes sharper and sharper because of the wall focusing effect which is a well-known phenomenon in laser

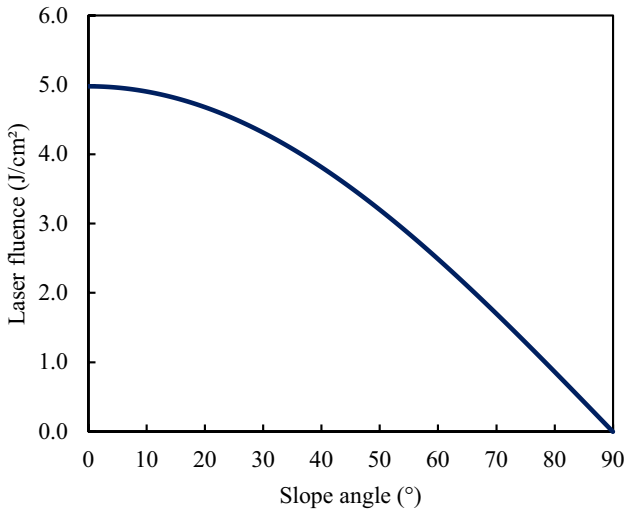

Fig. 6 Laser fluence change with slope angle

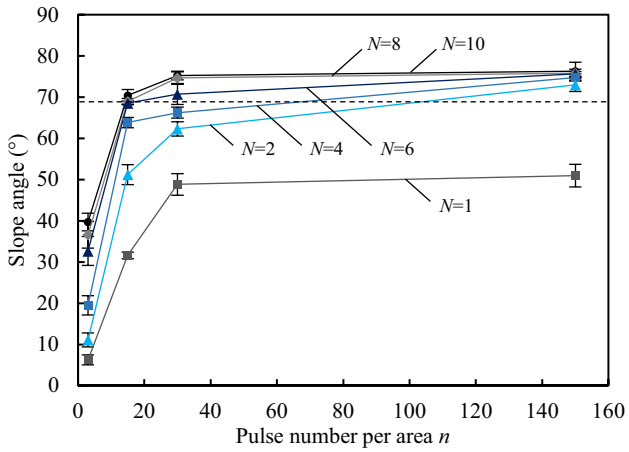

Fig. 8 Change in slope angle with pulse number per unit of area

drilling process [33, 34]. As shown in Fig. 7, the multiple incident light reflection phenomenon occurs at the groove walls and the reflected light gathers at the bottom. Then, the intensified laser induces further ablation, and as a result, a sharp corner is generated.

The final V-shaped groove slope angle depends on the laser scanning speed, as shown in Figs. 4 and 5. The scanning speed affects the number of pulses irradiated in per unit of area. To investigate this effect, the relationship between groove slope angle and pulse number per unit of area is summarized in Fig. 8. The pulse number per unit of area for a certain laser scanning speed was calculated by using the following equation:

$$n = \frac{d f}{v} \tag{3}$$

where v is scanning speed, d is laser spot diameter and f is laser frequency. In Fig. 8, the slope angle increases as pulse number increases when the pulse number is below 30. However, there is no significant change in slope angle when the pulse number is above 30. It indicates that the necessary pulse number to reach the ablation threshold is around 30. No change of slope angle occurs even increasing the total number of scans. In the early stage, each laser pulse causes ablation. Thus, as the pulse number increases, the slope angle increases too. However, as shown in Eq. (2), with the increase of the slope angle, the laser beam spot area becomes larger and the laser energy irradiated on per unit area (laser fluence) decreases. Once the laser fluence reaches below the ablation threshold, no further ablation will occur no matter how many pulses are irradiated at that fluence. As a result, the angle will not change even if the pulse number is increased further. In this study, it was observed that the laser fluence reached the ablation threshold when the

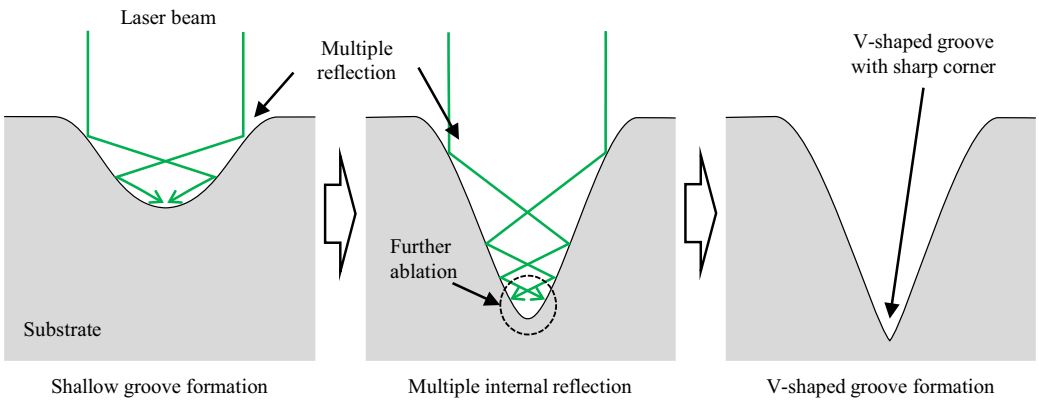

Fig. 7 Mechanism of V-shaped groove formation

pulse number was around 30, and the slope angle stopped increasing further. However, it should be pointed out that the critical pulse number depends on the workpiece material property and laser irradiation conditions, thus may change with laser parameters.

3.3 Phase Transformation

YSZ transforms from the tetragonal phase to the monoclinic phase due to thermal effect [2]. Since this phase transformation causes strength reduction of YSZ, it is necessary to restrain the phase transformation in laser processing. In this study, the peak intensities of the tetragonal and monoclinic phases were measured using a micro laser Raman spectrometer. Figure 9 shows the Raman spectra of the microgroove walls irradiated at different scanning speed with various number of scans. Before laser irradiation, two small monoclinic (m) peaks appeared on the original YSZ surface between the 147 and 264 cm^{-1} tetragonal (t) peaks. In case of 50 and 100 mm/s, these monoclinic peaks remained for a few repetitions of laser scan; however, they completely disappeared by further increasing the number of scans to $N \geq 2$ and $N \geq 5$, respectively. On the other hand, for a higher speed (500 mm/s), the monoclinic peaks did not disappear even when the number of scans increased to $N = 10$. From these results, it is found that different scanning speeds lead to different thresholds N. The decrease in the monoclinic peaks indicates the decrease of monoclinic phase in the YSZ sample, with tetragonal phase becoming more dominant. This result indicates the possibility of a laser-induced reverse transformation from the monoclinic phase to the tetragonal phase at the groove wall. By repeating laser scans, the monoclinic phase at the groove wall gradually changed to tetragonal phase, as a result, the monoclinic peak disappeared. The reverse phase transformation is further discussed in detail later in the paper.

For quantitative analysis of phase transformation, the monoclinic ratio V_m was calculated by the Raman intensity method [35]. Based on the results of Raman spectra, a baseline was drawn by connecting the minimum points between each peak. Then, integrated intensity I was measured for three peaks at 147, 181 and 190 cm^{-1}. From the Raman intensities, the monoclinic ratio V_m was calculated using Eq. (4) [35].

$$V_m = \frac{I_m(181) + I_m(190)}{2.07 \times I_t(147) + I_m(181) + I_m(190)} \tag{4}$$

where the subscripts m and t identify the monoclinic and tetragonal phases, respectively. Using monoclinic ratio V_m, we evaluated the phase transformation of YSZ after laser irradiation.

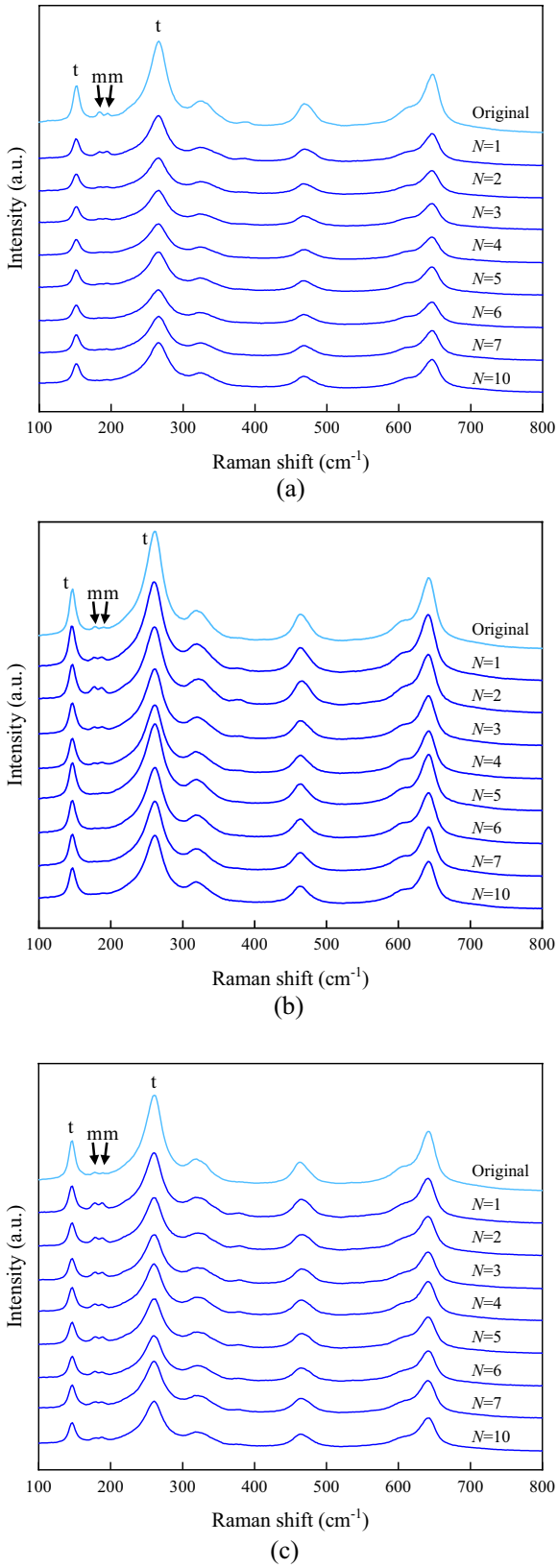

Fig. 9 Raman spectra of irradiated surface under various number of scans: **a** 50 mm/s, **b** 100 mm/s and **c** 500 mm/s

The calculated monoclinic ratio for each condition is shown in Fig. 10. Before laser treatment, the original YSZ sample had a monoclinic ratio of about 7%, as the original sample contained a small amount of monoclinic phase. In case of 100 mm/s, the monoclinic ratio became higher than the original surface when $N=2$, where the measurement error was quite big. On the other hand, monoclinic ratio decreased to 0.01 after 4 laser scans. For a lower speed (50 mm/s), the monoclinic ratio was higher than the original surface when $N=1$, however, the monoclinic ratio gradually decreased and became smaller than the unirradiated original surface with increasing the number of scans. On the other hand, for a higher speed of 500 mm/s, the monoclinic ratio was also larger than original surface after laser irradiation, although it tended to decrease slightly as the number of scans increased.

The drop of monoclinic ratio with increasing the number of scans may be attributed to three scenarios. First, it may be hypothesized that there is a relationship between groove slope angle and monoclinic ratio. According to the result of the change of microgroove slope angle shown in Fig. 5, in the case of 100 mm/s, the angle increased greatly when $N=1\sim4$, but there was almost no change when $N>4$. This means that no more energy absorption occurred at the groove wall when $N>4$. Therefore, the temperature change could not cause t-m phase transformation.

Another possible reason for the decrease in V_m after multiple irradiations is that the monoclinic phase generated in the first several times was removed in the following laser irradiations. Some researchers found that laser ablation can remove monoclinic phase from the sample, which is generated during the sample preparation process such as grinding and sand blasting [29, 36]. The removal of monoclinic phase from sample surface results in a lower monoclinic ratio than the original surface.

The third scenario may involve a m–t reverse transformation. Recent studies have shown that monoclinic phase can be transformed into tetragonal phase during cutting processes [23]. This reverse transformation is mainly induced by a local temperature change, and the m–t transformation temperature is about 1170 °C [2]. In laser irradiation process of this study, the monoclinic phase may transform to tetragonal.

Among the above three scenarios, the third one, i.e., the m–t reverse transformation may be the dominant reason for the drop of monoclinic ratio with increasing the number of laser scans. The Raman measurements were performed on the sides of the microgrooves at a depth of about 5 μm from the workpiece surface. If the monoclinic phase generated by previous irradiations is removed by subsequent irradiations, the monoclinic ratio should not change after the removal of the monoclinic layer, even if the number of scans increases. The fact that the monoclinic ratio gradually decreased with increasing the number of scans strongly indicates that a reverse phase transformation has occurred, and the monoclinic phase generated by previous irradiations is

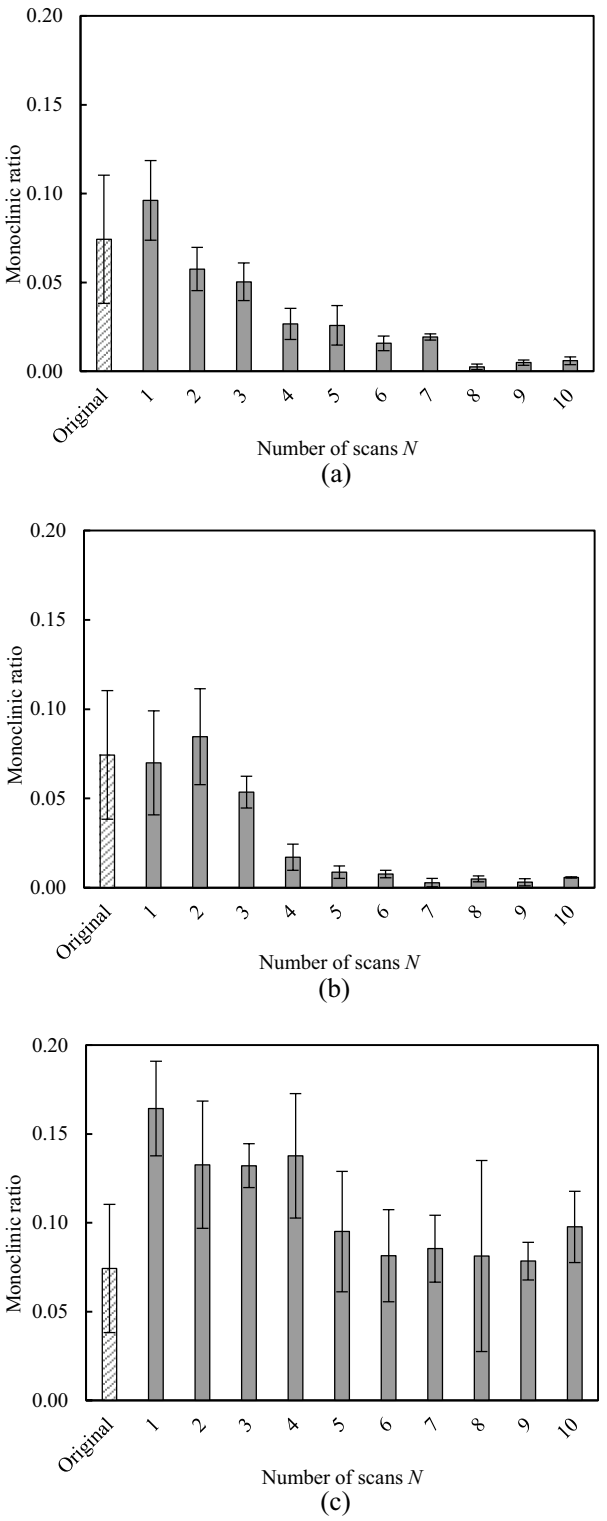

Fig. 10 Monoclinic ratio of irradiated surface under various number of scans: **a** 50 mm/s, **b** 100 mm/s and **c** 500 mm/s

gradually changed back to tetragonal phase by multiple irradiations. As the number of scans increases, the slope angle increases and the energy absorption decreases. As a result, the reverse phase transformation stops and the monoclinic ratio converges.

These results indicate that the effect of laser irradiation on m–t phase transformation is different with laser scanning speed. Since the overlap rate at 500 mm/s was much smaller (1/5th) than that at 100 mm/s, the maximum temperature which can be achieved and sustained is significantly lower due to reduced overlap rate. As temperature is most important factor for phase transformation to occur, temperature achieved at lower overlap rate (500 mm/s) was insufficient to cause reverse phase transformation.

3.4 Subsurface Microstructure

To investigate the subsurface structural change in detail, cross-sectional observation was performed for the grooves. Figure 11 shows the TEM images of the microgroove wall generated at a scanning speed of 100 mm/s with two different number of scans. For both $N=1$ and $N=10$, zirconia grains are clearly observed without microcracks and defects. In addition, zirconia grain boundary can be seen near the ablation boundary. The grain size is ~ 500 nm, which is the same as the original sample. The grains at the ablation boundary are separated and not connected with each other, indicating that the femtosecond pulsed laser irradiation led to a non-thermal material removal.

The SAED patterns of different areas are shown in Fig. 12. At the shallow area of the V-shaped groove wall (Fig. 12a–c), tetragonal planes (112), (101) and (211) were detected. Moreover, tetragonal phase was also observed in three different deep regions from the ablation boundary. Monoclinic pattern was not found at all. At the deeper area (Fig. 12d, e), the SAED pattern also showed tetragonal phase. These results are well consistent to the aforementioned results of monoclinic ratio calculated by Raman analysis. Phase transformation from tetragonal to monoclinic did not occur anywhere in the V-shaped groove. Therefore, in this study, it can be said ultrashort pulsed laser micro grooving does not trigger phase transformation from tetragonal to monoclinic inside the groove.

In general, there are two causes for phase transformation of zirconia, stress and temperature. When a tensile stress is applied to zirconia, t-m transformation occurs and

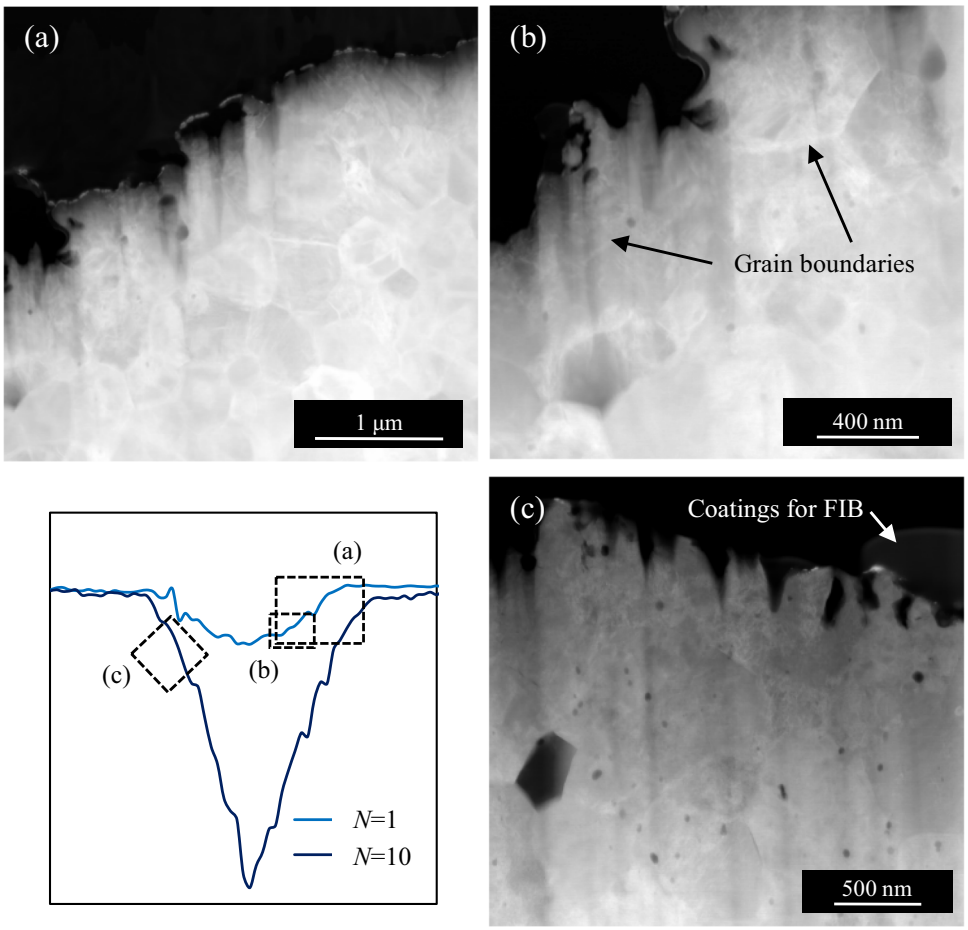

Fig. 11 TEM images of microgroove irradiated at various number of scans: **a** $N=1$, **b** $N=1$ at high magnification, and **c** $N=10$ (upper area)

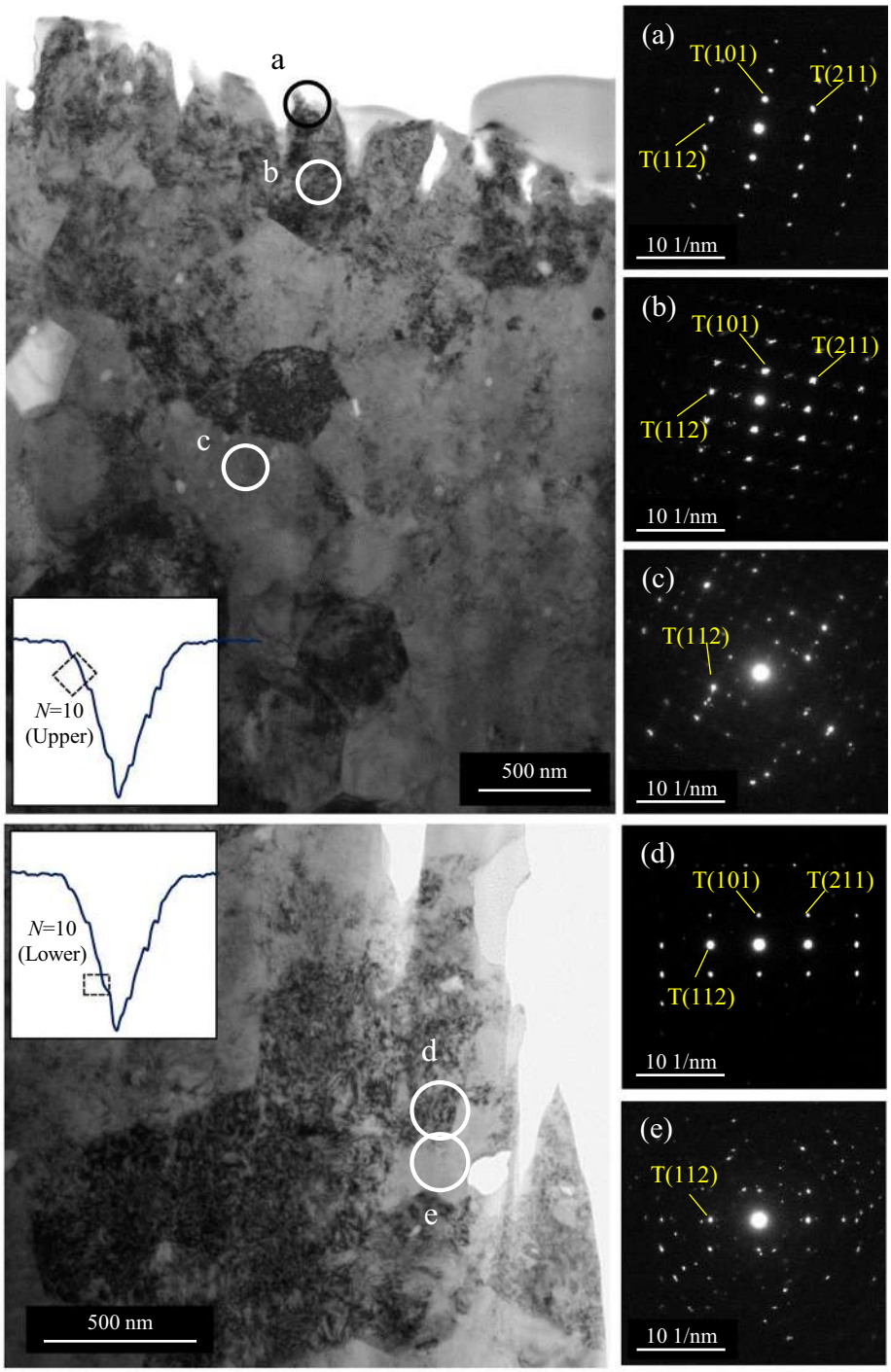

Fig. 12 TEM images and SAED patterns of cross-sectional microgroove irradiated at 100 mm/s: **a**–**c** upper area and **d**, **e** lower area (T indicates tetragonal)

induces volume expansion [3]. To reduce residual stress and realize m–t reverse phase transformation, thermal annealing is commonly used [23, 37]. In this study, no cracks and plastic deformation were found in the irradiated sample, which indicates that stress was not dominant during laser ablation process and the phase transformation was mainly caused by thermal effect.

In previous studies, femtosecond pulsed laser ablation did not induce a high amount of monoclinic phase [8, 29]. On the other hand, in the case of nanosecond pulsed irradiation, high localized thermal stress induced microcracks on laser treated surface which resulted in an increased amount of monoclinic phase [28, 37]. Even in case of

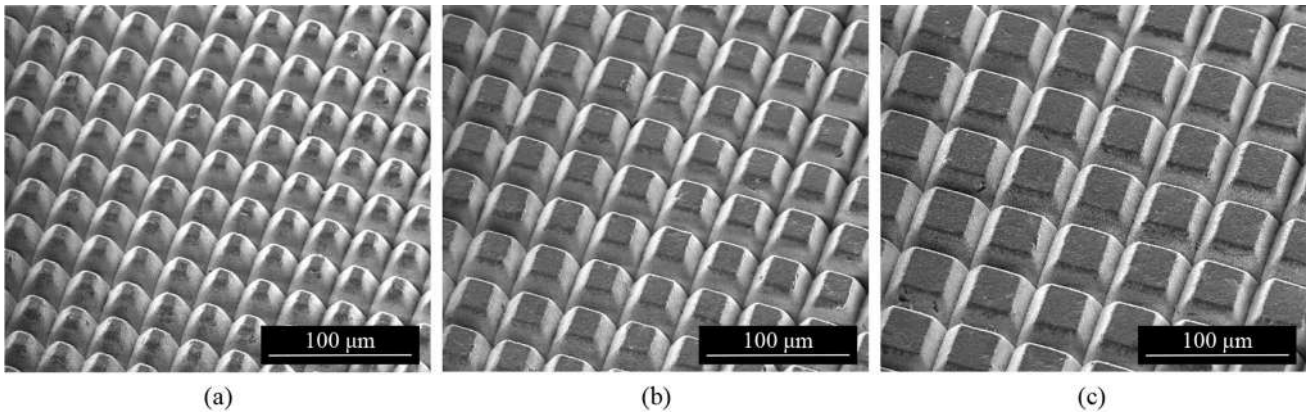

Fig. 13 SEM images of pyramidal structured surfaces with various pitches: **a** 30 µm, **b** 40 µm, and **c** 50 µm

picosecond pulsed laser, laser processing led to tetragonal to monoclinic phase transformation [38].

Most studies using femtosecond pulsed laser showed the possibility of reversing phase transformation to obtain a similar monoclinic ratio as the original surface, but there are no reports of reducing monoclinic ratio lower than the original surface as found in this study. It is hypothesized that in deep V-shaped grooves, heat accumulation occurred due to high density of plasma shielding and low thermal conductivity of zirconia [39]. Then by repeating laser scan, heating and cooling occurred, causing the transformation from monoclinic phase, which originally existed in the sample, to tetragonal phase.

3.5 Surface Patterning

Based on the results of micro V-shaped grooving, pyramid like structures were fabricated at a laser fluence of 5.0 J/cm^2, a scanning speed of 100 mm/s, and the laser was scanned for 10 cycles. Experimental condition was determined by minimizing the monoclinic ratio after laser treatment. According to the result of V-shaped groove width as shown in Fig. 4, the scanning pitch was set to be above 30 µm in order not to overlap the parallel V-shaped grooves.

The SEM images of the structures by various laser scanning pitches are shown in Fig. 13, and the corresponding cross-sectional profiles in Fig. 14. Pyramid structures were successfully generated on YSZ surfaces with precise V-shaped cross sections. There are no cracks and chippings on the surface, and sharp edges can be observed at crossing points of grooves. Moreover, compared with the aforementioned results of single V-shaped groove generation shown in Fig. 4, it is clear that the slope angles are uniform and precisely generated.

Three-dimensional surface topography of the pyramidal structures with a pitch of 30 µm is shown in Fig. 15. The tops of truncated pyramids had sharp edges, showing that the

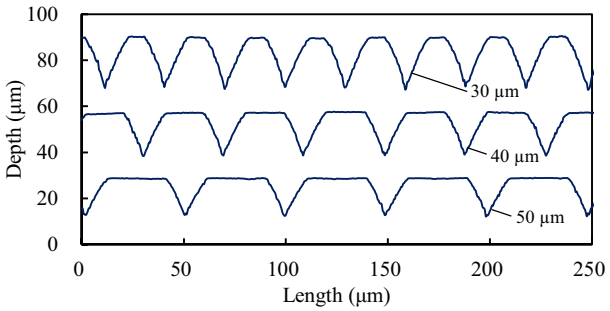

Fig. 14 Cross-sectional profiles of the pyramid structures

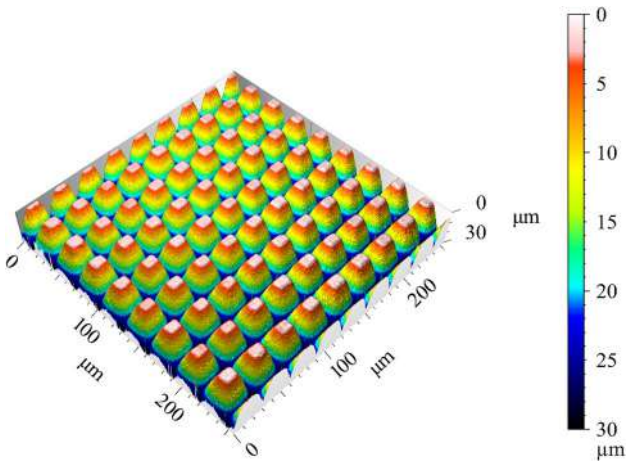

Fig. 15 Three-dimensional surface topography of pyramids with a pitch of 30 µm

original surface is partially remained on the top surface. The size of pyramid is limited by the laser spot size, as it limits the scanning pitch which can be used for creating pyramid surface structures. The limitation of the proposed process lies in two aspects, feature size and cross-sectional shape. As the size scale of the structure that can be fabricated by

laser processing is highly dependent on the spot diameter of the laser, grooves narrower than the spot diameter cannot be processed by this method. Regarding the cross-sectional shape of structures, V-grooves with various slope angles can be generated by this method through tilting the sample. It is also possible to fabricate high aspect grooves with vertical walls by tilting the sample to a suitable angle, as reported in one of our previous studies where vertical walls were made on sapphire surfaces [17]. However, the proposed method is not suitable for generating curved structures as the curvature control is difficult in laser processing.

3.6 Surface Wettability Change

As an example for investigation of the surface functionality, surface wettability of the micro textured zirconia surface was evaluated. The contact angles of the original sample and the laser-generated pyramidal structured surface were measured. A droplet of 5.0 μL pure water was used in a static sessile drop method at atmospheric condition.

Figure 16 shows the images of the water droplets on the original and pyramidal surface. The intrinsic contact angle of original YSZ surface is about 58°, thus the surface was hydrophilic. After surface structuring, the contact angle increased to above 90°, which indicates that surface was changed into a hydrophobic one. Figure 17 summarizes the change of contact angle with different pitches of micro pyramidal structures. Surface hydrophobicity was increased in all the specimens compared to the original surface, while the change in laser scanning pitch did not affect the contact angle significantly.

In general, surface wettability conditions can be classified into two states: Wenzel state where liquid penetrate the grooves and the contact area of liquid and substrate increases [40], and Cassie–Baxter state where air pocket is generated between the liquid and solid interface [41]. In the case of Wenzel regime, the wettability of original sample surface is enhanced due to the increase in contact area. However, in this study, the surface changed from hydrophilic to hydrophobic after laser surface patterning. Considering the

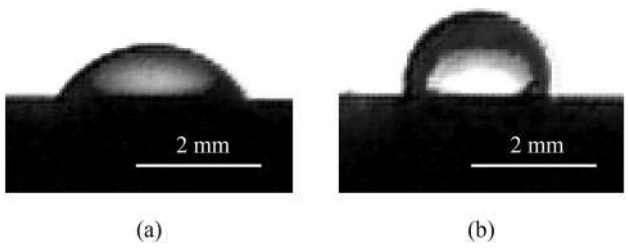

Fig. 16 Water droplets on unirradiated and pyramidal structured surfaces irradiated at a pitch of 30 μm: **a** original surface, and **b** pyramidal structured surfaces

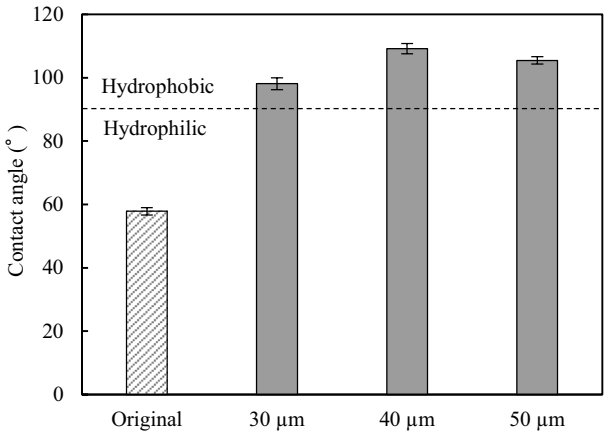

Fig. 17 Contact angle change of water droplets on original and pyramidal structured surfaces

Cassie–Baxter state, the apparent contact angle on a rough isotropic surface becomes hydrophobic regardless of original wettability of the material due to a significant decrease of contact area between droplets and sample surface. In this study, the pyramidal structures have led to hydrophobicity which is attributed to the dominance of the Cassie–Baxter state.

4 Conclusions

Femtosecond pulsed laser irradiation was performed on YSZ to investigate the fundamental micro grooving characteristics. The following conclusions were obtained.

(1) Micro V-shaped grooves with smooth sidewalls and sharp edges were generated by repeating line-scans of the laser beam. The groove depth strongly depends on the laser scanning speed.
(2) A V-shaped groove is developed as increasing the number of scans to a critical value (around 30 pulses per unit of area). Further increasing the number of scans did not change the taper angle and groove geometry.
(3) A tetragonal to monoclinic phase transformation was observed after laser irradiation. However, by increasing the number of scans, a reverse phase transformation from monoclinic to tetragonal occurred, leading to a monoclinic ratio lower than the original sample surface.
(4) Cross-sectional observation showed that grain boundaries were clearly remained under the ablated surface without melting. What's more important, crystal grains with tetragonal phase were observed regardless of the depth from groove wall.

(5) Three-dimensional pyramid microstructures were successfully fabricated, which change the original surface into hydrophobic.

This study showed the possibility of functionalization of YSZ surfaces by generating high aspect ratio microscale structures by using femtosecond pulsed laser irradiation. The slope angle and the geometry of the microstructures are controllable by laser irradiation parameters, and the resulting surface is free of thermal damage.

Declarations

Conflict of interest The authors declare that they have no known competing financial interests or personal relationships that could have appeared to influence the work reported in this paper.

References

1. Garvie, R. C., Hannink, R. H., & Pascoe, R. T. (1975). Ceramic steel? *Nature, 258*(5537), 703–704. https://doi.org/10.1038/258703a0
2. Scott, H. G. (1975). Phase relationships in the zirconia–yttria system. *Journal of Materials Science, 10*(9), 1527–1535. https://doi.org/10.1007/BF01031853
3. Gupta, T. K., Lange, F. F., & Bechtold, J. H. (1978). Effect of stress-induced phase transformation on the properties of polycrystalline zirconia containing metastable tetragonal phase. *Journal of Materials Science, 13*(7), 1464–1470. https://doi.org/10.1007/BF00553200
4. Piconi, C., & Maccauro, G. (1999). Zirconia as a ceramic biomaterial. *Biomaterials, 20*(1), 1–25. https://doi.org/10.1016/S0142-9612(98)00010-6
5. Sailer, I., Philipp, A., Zembic, A., Pjetursson, B. E., Hämmerle, C. H. F., & Zwahlen, M. (2009). A systematic review of the performance of ceramic and metal implant abutments supporting fixed implant reconstructions. *Clinical Oral Implants Research, 20*(SUPPL. 4), 4–31. https://doi.org/10.1111/j.1600-0501.2009.01787.x
6. Cho, G. Y., Yu, W., Lee, Y. H., Lee, Y., Tanveer, W. H., Kim, Y., Lee, S., Cha, S. W. (2020). Effects of nanoscale PEALD YSZ interlayer for AAO based thin film solid oxide fuel cells. *International Journal of Precision Engineering and Manufacturing Green Technology, 7*(2), 423–430. https://doi.org/10.1007/s40684-019-00082-9
7. Stanciuc, A. M., Flamant, Q., Sprecher, C. M., Alini, M., Anglada, M., & Peroglio, M. (2018). Femtosecond laser multi-patterning of zirconia for screening of cell-surface interactions. *Journal of the European Ceramic Society, 38*(3), 939–948. https://doi.org/10.1016/j.jeurceramsoc.2017.08.019
8. Carvalho, A., Cangueiro, L., Oliveira, V., Vilar, R., Fernandes, M. H., & Monteiro, F. J. (2018). Femtosecond laser microstructured alumina toughened zirconia: A new strategy to improve osteogenic differentiation of hMSCs. *Applied Surface Science, 435*, 1237–1245. https://doi.org/10.1016/j.apsusc.2017.11.206
9. Carvalho, A., Grenho, L., Fernandes, M. H., Daskalova, A., Trifonov, A., Buchvarov, I., & Monteiro, F. J. (2020). Femtosecond laser microstructuring of alumina toughened zirconia for surface functionalization of dental implants. *Ceramics International, 46*(2), 1383–1389. https://doi.org/10.1016/j.ceramint.2019.09.101
10. Ji, M., Xu, J., Chen, M., & El Mansori, M. (2020). Enhanced hydrophilicity and tribological behavior of dental zirconia ceramics based on picosecond laser surface texturing. *Ceramics International, 46*(6), 7161–7169. https://doi.org/10.1016/j.ceramint.2019.11.210
11. Chen, F., Zhang, D., Yang, Q., Yong, J., Du, G., Si, J., Yun, F., Hou, X. (2013). Bioinspired wetting surface via laser microfabrication. *ACS Applied Materials and Interfaces, 5*(15), 6777–6792. https://doi.org/10.1021/am401677z
12. Yao, L., & He, J. (2014). Recent progress in antireflection and self-cleaning technology—From surface engineering to functional surfaces. *Progress in Materials Science, 61*, 94–143. https://doi.org/10.1016/j.pmatsci.2013.12.003
13. Yan, J., & Okuuchi, T. (2019). Chip morphology and surface integrity in ultraprecision cutting of yttria-stabilized tetragonal zirconia polycrystal. *CIRP Annals, 68*(1), 53–56. https://doi.org/10.1016/j.cirp.2019.04.050
14. Holthaus, M. G., Twardy, S., Stolle, J., Riemer, O., Treccani, L., Brinksmeier, E., & Rezwan, K. (2012). Micromachining of ceramic surfaces: Hydroxyapatite and zirconia. *Journal of Materials Processing Technology, 212*(3), 614–624. https://doi.org/10.1016/j.jmatprotec.2011.06.007
15. Lu, A., Gao, Y., Jin, T., Luo, X., Zeng, Q., & Shang, Z. (2020). Effects of surface roughness and texture on the bacterial adhesion on the bearing surface of bio-ceramic joint implants: An in vitro study. *Ceramics International, 46*(5), 6550–6559. https://doi.org/10.1016/j.ceramint.2019.11.139
16. Smielak, B., & Klimek, L. (2015). Effect of hydrofluoric acid concentration and etching duration on select surface roughness parameters for zirconia. *Journal of Prosthetic Dentistry, 113*(6), 596–602. https://doi.org/10.1016/j.prosdent.2015.01.001
17. Takayama, N., Asaka, S., & Yan, J. (2018). Nanosecond pulsed laser irradiation of sapphire for developing microstructures with deep V-shaped grooves. *Precision Engineering, 52*(February), 440–450. https://doi.org/10.1016/j.precisioneng.2018.02.008
18. Aguilar-Morales, A. I., Alamri, S., & Lasagni, A. F. (2018). Micro-fabrication of high aspect ratio periodic structures on stainless steel by picosecond direct laser interference patterning. *Journal of Materials Processing Technology, 252*, 313–321. https://doi.org/10.1016/j.jmatprotec.2017.09.039
19. Fiedler, S., Irsig, R., Tiggesbäumker, J., Schuster, C., Merschjann, C., Rothe, N., Lochbrunner, S., Vehse, M., Seitz, H., Klinkenberg, E.-D., Meiwes-Broer, K.-H. (2013). Machining of biocompatible ceramics with femtosecond laser pulses. *Biomedical Engineering Biomedizinische Technik, 58*, 3–4. https://doi.org/10.1515/bmt-2013-4093
20. Kim, M., Lee, S. M., Lee, S. J., Kim, Y. W., Liang-Li, & Lee, D. W. (2017). Effect on friction reduction of micro/nano hierarchical patterns on sapphire wafers. *International Journal of Precision Engineering and Manufacturing Green Technology, 4*(1), 27–35. https://doi.org/10.1007/s40684-017-0004-3
21. Wang, X. C., Wu, L. Y. L., Shao, Q., & Zheng, H. Y. (2009). Laser micro structuring on a Si substrate for improving surface hydrophobicity. *Journal of Micromechanics and Microengineering, 19*(8), 085025. https://doi.org/10.1088/0960-1317/19/8/085025
22. Chevalier, J., Gremillard, L., Virkar, A. V., & Clarke, D. R. (2009). The tetragonal-monoclinic transformation in zirconia: Lessons learned and future trends. *Journal of the American Ceramic Society, 92*(9), 1901–1920. https://doi.org/10.1111/j.1551-2916.2009.03278.x
23. Grigore, A., Spallek, S., Petschelt, A., Butz, B., Spiecker, E., & Lohbauer, U. (2013). Microstructure of veneered zirconia after surface treatments: A TEM study. *Dental Materials, 29*(11), 1098–1107. https://doi.org/10.1016/j.dental.2013.07.022

24. Feng, D., & Shen, H. (2019). Hole quality control in underwater drilling of yttria-stabilized zirconia using a picosecond laser. *Optics and Laser Technology, 113*, 141–149. https://doi.org/10.1016/j.optlastec.2018.12.019
25. Li, J., Ji, L., Hu, Y., & Bao, Y. (2016). Precise micromachining of yttria-tetragonal zirconia polycrystal ceramic using 532 nm nanosecond laser. *Ceramics International, 42*(3), 4377–4385. https://doi.org/10.1016/j.ceramint.2015.11.118
26. Roitero, E., Anglada, M., Mücklich, F., & Jiménez-Piqué, E. (2018). Mechanical reliability of dental grade zirconia after laser patterning. *Journal of the Mechanical Behavior of Biomedical Materials, 86*(June), 257–263. https://doi.org/10.1016/j.jmbbm.2018.06.039
27. Cai, Y., Chang, W., Luo, X., & Qin, Y. (2019). Superhydrophobicity of microstructured surfaces on zirconia by nanosecond pulsed laser. *Journal of Micromanufacturing, 2*(1), 5–14. https://doi.org/10.1177/2516598418799933
28. Roitero, E., Lasserre, F., Roa, J. J., Anglada, M., Mücklich, F., & Jiménez-Piqué, E. (2017). Nanosecond-laser patterning of 3Y-TZP: Damage and microstructural changes. *Journal of the European Ceramic Society, 37*(15), 4876–4887. https://doi.org/10.1016/j.jeurceramsoc.2017.05.052
29. Delgado-Ruíz, R. A., Calvo-Guirado, J. L., Moreno, P., Guardia, J., Gomez-Moreno, G., Mate-Sánchez, J. E., Ramirez-Fernández, P., Chiva, F. (2011). Femtosecond laser microstructuring of zirconia dental implants. *Journal of Biomedical Materials Research Part B Applied Biomaterials, 96 B*(1), 91–100. https://doi.org/10.1002/jbm.b.31743
30. Ackerl, N., & Wegener, K. (2019). Ablation characteristics of alumina and zirconia ceramics on ultra-short pulsed laser machining. *Journal of Laser Micro Nanoengineering, 14*(2), 168–172. https://doi.org/10.2961/jlmn.2019.02.0009
31. Bonse, J., Hohm, S., Kirner, S. V., Rosenfeld, A., & Kruger, J. (2017). Laser-induced periodic surface structures—A scientific evergreen. *IEEE Journal of Selected Topics in Quantum Electronics, 23*(3), 109–123. https://doi.org/10.1109/JSTQE.2016.2614183
32. Jing, X., Pu, Z., Zheng, S., Wang, F., & Qi, H. (2020). Nanosecond laser induced microstructure features and effects thereof on the wettability in zirconia. *Ceramics International, 46*(15), 24173–24182. https://doi.org/10.1016/j.ceramint.2020.06.197
33. Milewski, J., & Sklar, E. (1996). Modelling and validation of multiple reflections for enhanced laser welding. *Modelling and Simulation in Materials Science and Engineering, 4*(3), 305–322. https://doi.org/10.1088/0965-0393/4/3/005
34. Samant, A. N., & Dahotre, N. B. (2009). Laser machining of structural ceramics—A review. *Journal of the European Ceramic Society, 29*(6), 969–993. https://doi.org/10.1016/j.jeurceramsoc.2008.11.010
35. Muñoz Tabares, J. A., & Anglada, M. J. (2010). Quantitative analysis of monoclinic phase in 3Y-TZP by Raman spectroscopy. *Journal of the American Ceramic Society, 93*(6), 1790–1795. https://doi.org/10.1111/j.1551-2916.2010.03635.x
36. Kosmač, T., Oblak, Č, & Marion, L. (2008). The effects of dental grinding and sandblasting on ageing and fatigue behavior of dental zirconia (Y-TZP) ceramics. *Journal of the European Ceramic Society, 28*(5), 1085–1090. https://doi.org/10.1016/j.jeurceramsoc.2007.09.013
37. Roitero, E., Ochoa, M., Anglada, M., Mücklich, F., & Jiménez-Piqué, E. (2018). Low temperature degradation of laser patterned 3Y-TZP: Enhancement of resistance after thermal treatment. *Journal of the European Ceramic Society, 38*(4), 1742–1749. https://doi.org/10.1016/j.jeurceramsoc.2017.10.044
38. Yamamuro, Y., Shimoyama, T., Yamashita, I., & Yan, J. (2020). Multiscale surface patterning of zirconia by picosecond pulsed laser irradiation. *Journal of Micro and Nano-Manufacturing, 8*(1), 8–13. https://doi.org/10.1115/1.4046040
39. Raghavan, S., Wang, H., Dinwiddie, R. B., Porter, W. D., & Mayo, M. J. (1998). The effect of grain size, porosity and yttria content on the thermal conductivity of nanocrystalline zirconia. *Scripta Materialia, 39*(8), 1119–1125. https://doi.org/10.1016/S1359-6462(98)00290-5
40. Wenzel, R. N. (1936). Resistance of solid surfaces to wetting by water. *Industrial and Engineering Chemistry, 28*(8), 988–994. https://doi.org/10.1021/ie50320a024
41. Cassie, A. B. D., & Baxter, S. (1944). Wettability of porous surfaces. *Transactions of the Faraday Society, 40*, 546–551. https://doi.org/10.1039/tf9444000546

Yuka Yamamuro received her Bachelor's degree in Mechanical Engineering from Keio University in 2019. She is currently a Master degree student at Keio University, starting Ph.D. study in Mechanical Engineering under supervision of Prof. Yan. Her research interests include laser processing and micro/nano manufacturing.

Tomotaka Shimoyama received his Ph.D. in Science from Tokyo Institute of Technology, Japan in 2008. He is currently a group leader of Inorganic Materials Research Laboratory, TOSOH Corporation (2019–now). His research interest includes crystallography of inorganic materials and condensed matter physics.

Jiwang Yan received his Ph.D. from Tohoku University, Japan in 2000 and is currently a professor of Mechanical Engineering at Keio University (2012–now), leading the Laboratory for Precision Machining and Nano Processing. His research areas include ultraprecision machining, micro manufacturing, nanomaterial processing, and nanomechanics.